Coverage dependence and surface atomic structure of Mn/Si(111)-$\sqrt{3}\times\sqrt{3}$ studied by scanning tunneling microscopy and spectroscopy

J. Hirvonen Grytzelius,* H. M. Zhang, and L. S. O. Johansson
Department of Physics, Karlstad University, S-651 88 Karlstad, Sweden
(Received 16 June 2009; revised manuscript received 19 November 2009; published 18 December 2009)

Thin manganese silicide films of different thicknesses on Si(111) have been studied in detail by low-energy electron diffraction (LEED), scanning tunneling microscopy, and scanning tunneling spectroscopy (STM/STS). Up to a Mn coverage of 3–4 monolayers (ML), island formation is favored. For higher Mn coverages up to 12 ML uniform film growth is found. The silicide film morphology at low coverages supports a layered Mn-Si film structure. The silicide surfaces displayed a $\sqrt{3}\times\sqrt{3}$ LEED pattern. STM images recorded from the $\sqrt{3}\times\sqrt{3}$ surfaces mostly show a hexagonal pattern but a honeycomb pattern has also been observed. A surface atomic structure based on chained Mn triangles is proposed. Our STM results are in good agreement with a recent theoretical model. The high-quality STS spectra recorded from the different surfaces show a clear metallic character at 1.5 ML and higher coverages. The filled-state features in the STS spectra at surfaces with 3–4 ML Mn coverages are similar to earlier published angle-resolved photoelectron spectroscopy data.

DOI: 10.1103/PhysRevB.80.235324 PACS number(s): 68.37.Ef, 68.35.bg, 68.35.bj

I. INTRODUCTION

New materials possessing both semiconducting and magnetic properties are of great interest both from technological aspects and from a fundamental physics point of view. The combination of these two large branches of physics could lead to great improvements in the modern technological field. Using the spin degree of freedom of the electron in the standard charge-based electronics will improve data storage and memory handling.[1] It is, however important to understand the fundamental properties of those materials that are candidates for applications in the field of spintronics.

Mn on Si(111) does not have a simple adatom reconstruction.[2] Instead, a layered Mn-silicide structure has been suggested by Tanaka *et al.*[3] and Hortamani *et al.*[4] Earlier studies have focused on growth and morphology of ultrathin Mn films on Si(111), reporting dependence on temperature and deposition rate.[5,6] Higashi *et al.*[7,8] observed flat manganese silicide films having a *B*20 structure with a thickness of 7 Å. Both Volmer-Weber and Frank-van der Merwe growth modes have been reported for the Mn-silicide film.[2,5] The growth properties of thick Mn-silicide films, up to 100 Å, have also been studied.[9–12] Epitaxially grown silicide films have been investigated by x-ray absorption, Auger, core-level, and valence-band spectroscopies,[13–17] showing a strain dislocation in the film at a coverage of 5 monolayers (ML).[16] So far there is only a few reports dealing with the surface atomic structure of the Mn/Si(111)-$\sqrt{3}\times\sqrt{3}$ film, all suggesting a surface terminated by silicon atoms.[3,4,16]

In this paper we present our experimental results regarding the film morphology, atomic structure, and electronic properties of thin solid phase epitaxy grown MnSi films with a Mn content from 1.5 to 12 ML. The surfaces have been investigated in detail by scanning tunneling microscopy and spectroscopy (STM/STS). The film morphology at low Mn coverages reveals a layered silicide structure, in good quantitative agreement with a recent theoretical model.[4] We investigate in detail the atomic and electronic structure of the well-ordered $\sqrt{3}\times\sqrt{3}$ reconstruction on the surfaces of the MnSi films. We show that the surface reconstruction can be described by atoms arranged in triangular structures, in close analogy to the Ag/Si(111)-$\sqrt{3}\times\sqrt{3}$ surface, and in agreement with theory.[4]

II. EXPERIMENTAL DETAILS

The STM study was performed in a variable-temperature STM system from Omicron Nanotechnology GmbH. The STM tip was made from a *W* wire. Si(111) samples were cut from commercially available single-crystal wafers into a size of 3×10 mm^2 to fit the sample holder. The samples were precleaned by an etching method and outgassed *in situ* by direct current heating at 600 °C for several hours. This was followed by stepwise heating up to 930 °C and then by rapid flash heating up to 1230 °C. The procedure resulted in well-ordered 7×7 surfaces as seen by both low-energy electron diffraction (LEED) and STM. The annealing temperatures were measured with infrared pyrometers.

Manganese were evaporated from a well-outgassed electron-beam evaporator (Omicron/Focus) onto clean and well-ordered Si(111)-7×7 surfaces at a rate of 0.5 ML/min, where 1 ML is defined as the number of the topmost atoms in the unreconstructed Si(111) surface (1 ML=7.83×10^{14} atoms/cm^2). The evaporator was carefully calibrated by a quartz-crystal-thickness monitor. The pressure during evaporation was lower than 2×10^{-10} and $\sim6\times10^{-11}$ mbar during measurements.

After Mn deposition, the 1.5 ML sample was probed with STM and thereafter annealed in several steps. First, the annealing was done at 300 °C and stopped when a 1×1 diffraction pattern was observed by LEED [Fig. 1(a)]. The 1×1 surface was scanned by STM before it was further annealed at 400 °C for 5 min. After annealing, intense 1×1 diffraction spots together with weak $\sqrt{3}\times\sqrt{3}$ and 2×2 diffraction spots were seen by LEED [Fig. 1(b)]. When the annealing temperature was slowly increased above 400 °C, new 7×7 diffraction spots appeared in LEED besides the

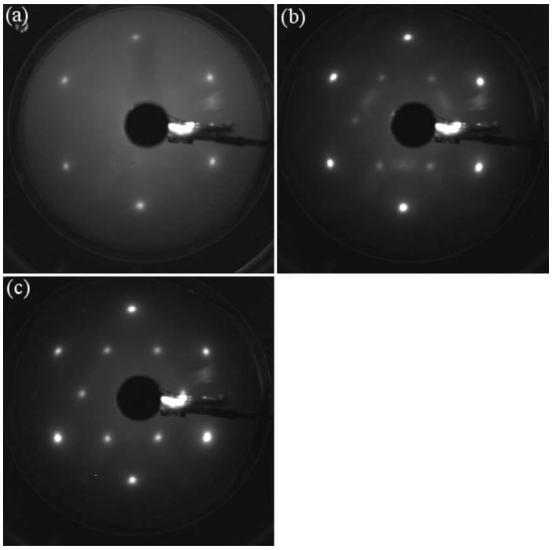

FIG. 1. LEED patterns of Mn/Si(111) surfaces as a function of annealing temperature and Mn coverages; (a) 1.5 ML annealed at 300 °C showing a 1×1 pattern; (b) 1.5 ML annealed at 400 °C for 5 min showing a weak $\sqrt{3}\times\sqrt{3}$ pattern; and (c) 4 ML annealed at 400 °C for 5 min showing a strong $\sqrt{3}\times\sqrt{3}$ pattern. All images were recorded at 46 eV.

2×2 and $\sqrt{3}\times\sqrt{3}$ diffraction spots. After annealing at 450 °C for 5 min, overlapping $\sqrt{3}$ and a clear 7×7 diffraction patterns were seen by LEED but no traces from the 2×2 spots.

The 3, 4, and 12 ML samples were annealed at 400 °C for 5 min. The resulting LEED patterns showed intense 1×1 and $\sqrt{3}\times\sqrt{3}$ diffraction spots. In Fig. 1(c), the LEED image from the 4 ML sample is presented.

All STM images in this paper were recorded in constant current mode. The STS spectra were recorded with the feedback loop turned off.

III. RESULT AND DISCUSSION

In Figs. 2(a) and 2(b), the STM results from the as-deposited 1.5 ML sample are shown. It is clear from Fig. 2(a) that the manganese is uniformly distributed in small clusters over the substrate. A step edge from the Si(111) substrate is clearly seen in the image. A closeup image from this surface is shown in Fig. 2(b). The average diameter of the small Mn clusters is estimated to ~30 Å.

In Figs. 2(c) and 2(d), topographic STM images recorded from the 1.5 ML sample annealed at 300 °C are shown. Figure 2(c) shows an overview from the surface that produced the 1×1 LEED pattern in Fig. 1(a). Clearly, the uniformly distributed Mn clusters observed for the as-deposited sample have migrated over the surface and formed large flat islands. Beside the larger islands unreacted Mn clusters are still observed as well as traces from the 7×7 surface and 2×2 structures. In Fig. 2(d) a closeup image from one of the flat islands is shown. The height of the island is estimated to 5 Å and the diameter to 15 nm. The surface of the island has a well-ordered $\sqrt{3}\times\sqrt{3}$ reconstruction. These observations

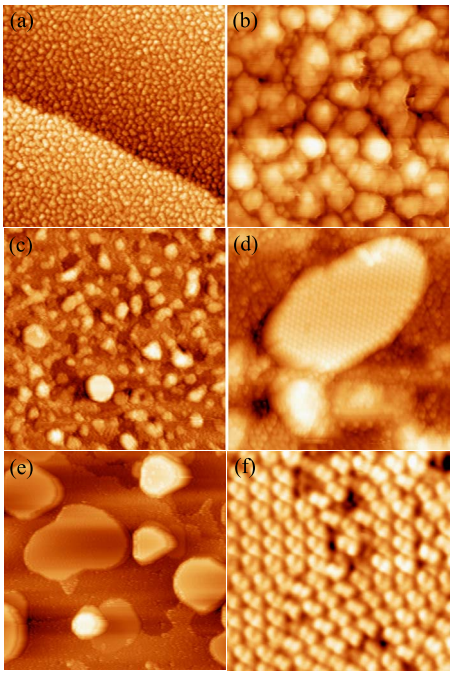

FIG. 2. (Color online) Topographic STM images from the 1.5 ML sample. (a) and (b) show large and small scale images from the as-deposited sample, 100×100 nm^2 and 20×20 nm^2, respectively. Both images were recorded at $V_S=1.6$ V and $I=0.2$ nA. (c) Image after anneal at ~300 °C, $V_S=-1.6$ V, $I=1$ nA, and 100×100 nm^2. (d) Closeup image of one of the islands seen in (c), $V_S=-1.5$ V, $I=0.2$ nA, and 25×25 nm^2. (e) A 100×100 nm^2 image showing MnSi islands from the 1.5 ML sample annealed at 400 °C. (f) An 8×8 nm^2 image showing the $2\times$ regions from the areas between the islands in (e). [(e) and (f)] $V_S=1.5$ V and $I=0.1$ nA.

show that the $\sqrt{3}$ phase starts to form already at 300 °C which is consistent with the findings of Ref. 2.

Figure 2(e) shows a topographic image obtained from the 1.5 ML sample annealed at 400 °C. Here, flat islands are observed with an averaged diameter of ~25 nm. These islands have a well-ordered $\sqrt{3}\times\sqrt{3}$ reconstructed surface. The coverage of the $\sqrt{3}\times\sqrt{3}$ phase estimated from the image-processing software[18] is ~35%. The heights of the islands are between 6 and 15 Å. In Fig. 2(f) a closeup image from the area between the islands is shown. This area has a dominating 2×2 reconstruction. As stated above, the $\sqrt{3}\times\sqrt{3}$ and 2×2 regions also appear as extra weak spots in the LEED image [Fig. 1(b)].

After annealing at 450 °C for 5 min, both $\sqrt{3}$ and 7×7 LEED diffraction spots were seen. This was confirmed by the STM images (not shown) where most of the areas between the islands exhibited a 7×7 reconstruction. Also, the number of islands decreased while their height increased to an average value of ~15 Å. This shows that the recrystallization of the 7×7 surface starts to occur at a temperature just above 400 °C. At a temperature of 450 °C most of the areas between the islands that possessed a 2×2 reconstruction have transformed into the 7×7 reconstruction.

In Fig. 3(a) a large-scale image from the 3 ML sample is shown. All the bright areas exhibit a very well-ordered $\sqrt{3}$

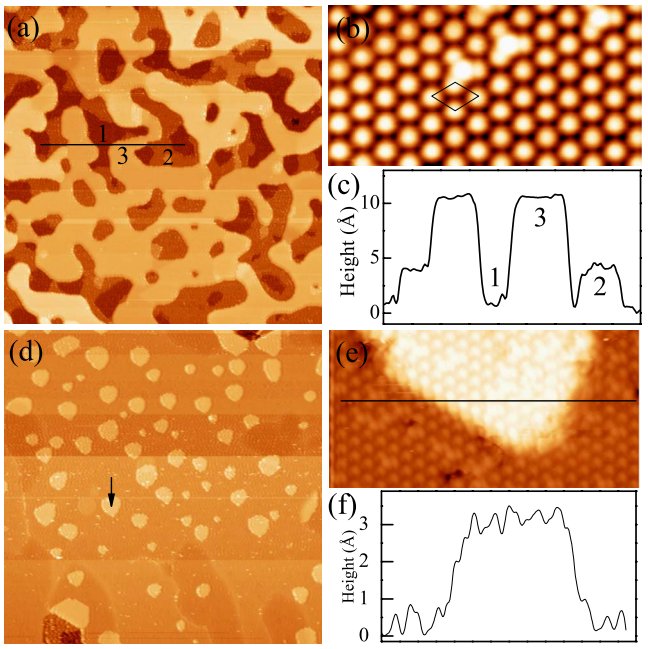

FIG. 3. (Color online) Topographic STM images from the Mn/Si(111) surfaces. (a) A 200×200 nm^2 image from the annealed 3 ML sample, V_S=1.6 V and I=0.5 nA. (b) 8×4 nm^2 image from the $\sqrt{3}\times\sqrt{3}$ surface in (a), V_S=−1.4 V and I=0.05 nA. (c) Line profile along the black line in (a) showing the height difference between the layers. (d) A 200×200 nm^2 image from the 4 ML sample, V_S=−0.9 V and I=0.2 nA. (e) A 14×7 nm^2 image from the surface in (d), V_S=0.9 V and I=0.3 nA. (f) Line profile along the black line in (e) showing the island height.

$\times\sqrt{3}$ reconstruction. A small-scale image is shown in Fig. 3(b). The white protrusions form a perfect $\sqrt{3}\times\sqrt{3}$ reconstructed surface as indicated by the plotted unit cell. Also, extra white protrusions on top of this surface are seen. They are located in the middle between three $\sqrt{3}$ protrusions and have a threefolded symmetry. The amount of extra protrusions (compared to $\sqrt{3}$ protrusions) is estimated to be a few percent (~7%).

A line profile is drawn along the black line in Fig. 3(a) and is shown in Fig. 3(c). There are three main areas of terraces of interest; these are marked by numbers in each figure. The first terrace, marked 1, is the deepest and shows a disordered structure. The coverage of this phase is ~10% of the surface area. The second terrace, marked 2, has a coverage ~15% and shows $2\times$ structures similar to that observed for the 1.5 ML sample. The measured height difference between terraces 1 and 2 is ~3 Å. The third terrace, marked 3, with the well-ordered $\sqrt{3}$ periodicity has a coverage of ~70–75%. The height difference between terraces 2 and 3 is ~6.8 Å.

It is interesting to compare our measurements with the theoretical model presented by Hortamani *et al.* [Figs. 1(c)–1(d) in Ref. 4]. The measured height between terraces 2 and 3 corresponds well with two quadruple layers with a thickness of ~5.4 Å (where one quadruple layer consists of a sparse Mn, sparse Si, dense Mn, and a dense Si layer, see description in Ref. 4) plus one extra dense Si layer at the interface between the substrate and the film. Also, the height difference between terraces 1 and 2 (3 Å) fits well with a Si bilayer distance (3.1 Å). It seems reasonable to assign terrace 1 to the bare substrate, one bilayer below the top Si layer. Terrace 2 is assigned to the top Si layer possessing a 2×2 reconstruction, and terrace 3 to one dense Si layer and two quadruple layers above the top Si layer of terrace 2.

After annealing the 4 ML sample at 400 °C for 5 min the surface was fully covered with a well-ordered $\sqrt{3}\times\sqrt{3}$ structure. Figure 3(d) shows a topographic image from this surface. On top of the surface flat islands are observed, all having a well-ordered $\sqrt{3}$ periodicity. One of these islands is indicated by an arrow in Fig. 3(d) and a closeup image of parts of it is shown in Fig. 3(e). A line profile is drawn along the black line in Fig. 3(e) and is shown in Fig. 3(f). The height difference between the island and the film is 2.8 Å. This height is close to one quadruple layer (2.7 Å) and is an indication of a third layer of MnSi. The average diameter of the islands seen in Fig. 3(d) is ~10 nm.

Up to a coverage of 3–4 ML and an annealing temperature of 400 °C island formation is favored. At 4 ML coverage a few deep holes are observed in the film with a depth between ~8–14 Å. The depth can be related to film thicknesses of two or three quadruple layers with a dense Si layer at the interface between the film and the substrate. These holes were considered by Ref. 16 to be either the feedstock with silicon for further silicide formation or acting as local strain relief in the film. We notice that the ideal $\sqrt{3}$ film is between 3 and 4 ML Mn, which is slightly higher than the value found in our previous study.[15]

One sample with a coverage of 12 ML Mn was also prepared for comparison (data not shown). The LEED image recorded for this sample showed intense $\sqrt{3}\times\sqrt{3}$ diffraction spots similar to that observed for the 3 and 4 ML samples. At this coverage the whole surface has a very well-ordered $\sqrt{3}\times\sqrt{3}$ reconstruction. Also this surface has the extra white protrusions on top, located between three white protrusions. By measuring the corrugation along the surface, steps with an height of 2.8 Å, is observed which corresponds well to one quadruple layer. Apparently the surface termination seems to be the same for the 3, 4, and 12 ML films as well as for the islands from the 1.5 ML sample.

To conclude this part, the morphology of the MnSi films at 3 and 4 ML Mn coverages indicates a layered structure of the silicide film. The heights of the terraces are in good quantitative agreement with the theoretical model presented in Ref. 4.

A more detailed investigation of the $\sqrt{3}\times\sqrt{3}$ surface from the 3 ML sample is shown in Figs. 4(a)–4(c). The $\sqrt{3}\times\sqrt{3}$ unit cell is indicated by the white unit cells in each figure. It should be noted that the unit cells in Figs. 4(a)–4(c) are carefully placed at the same surface location. In Figs. 4(a) and 4(b) the empty- and filled-state images, respectively, are shown from the $\sqrt{3}\times\sqrt{3}$ surface. The images seem quite similar, except that in the empty-state image [Fig. 4(a)] the white protrusions appear more intense compared to the protrusions in the filled-state image [Fig. 4(b)].

When scanning the same area under the same conditions we mostly observed a hexagonal pattern [Fig. 4(a)] but also a honeycomb pattern was found occasionally [Fig. 4(c)]. The hexagonal pattern is observed when one bright protrusion is

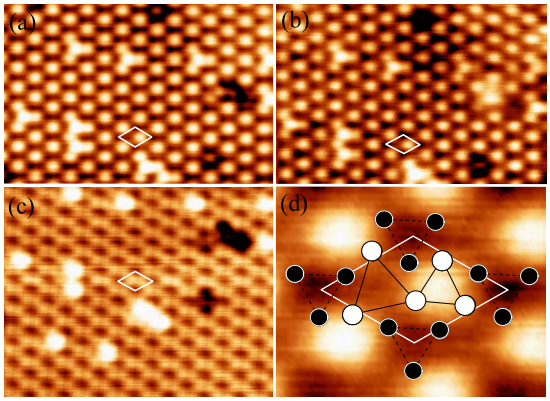

FIG. 4. (Color online) STM images from the Mn/Si(111)-$\sqrt{3}\times\sqrt{3}$ surface with 3 ML coverage. (a) Empty-state image recorded at V_S=1.6 V, I=1.5 nA, and 9×6 nm^2. (b) Filled-state image from the same area as in (a), V_S=−1.6 V, I=1.5 nA, and 9×6 nm^2. (c) Empty-state image recorded from the same area and at the same conditions as in (a), 9×7 nm^2. (d) Top view of the IET atomic structure of the $\sqrt{3}\times\sqrt{3}$ surface, 1.8×1.2 nm^2. White and black circles correspond to Mn and Si atoms, respectively.

seen to the right in the $\sqrt{3}\times\sqrt{3}$ unit cell. When the honeycomb pattern is observed, two bright protrusions are seen on each side of the $\sqrt{3}\times\sqrt{3}$ unit cell.

The observation of both hexagonal and honeycomb patterns is similar to what has been observed for the Ag/Si(111)-$\sqrt{3}\times\sqrt{3}$ surface.[19] As discussed in Ref. 19, the observation of either a honeycomb or a hexagonal pattern for the same tunneling conditions, is caused by a tip reconstruction which in turn changes the wave function on the tip apex. Consequently, the tip becomes sensitive to certain surface electronic structures. The tip reconstruction may be caused by the pickup of atoms from the surface.

The observation of a honeycomb pattern in the Ag/Si(111)-$\sqrt{3}\times\sqrt{3}$ case has been explained by a honeycomb-chain-trimer (HCT) model. In that model, a Si trimer is surrounded by six chained Ag trimers, located at the corners of the honeycomb hexagons in the STM image, which form the honeycomb pattern. The observation of a hexagonal pattern is instead explained by an inequivalent triangle (IET) model. The IET model differs from the HCT model by a small rotation and displacement of the Ag atoms. The result is a small and a large Ag trimer, where the small Ag trimer appears bright and the large Ag trimer appears darker in the STM image. The detailed models can be found in Fig. 1 of Ref. 19. As discussed in that paper, depending on the condition of the tip, the images display either the states located at all Ag trimers or preferentially only states located on the small Ag trimers, giving rise to the honeycomb and hexagonal patterns, respectively.

The close similarity between the present case and the Ag/Si(111)-$\sqrt{3}\times\sqrt{3}$ case regarding the observation of both a hexagonal and a honeycomb pattern, suggests that the Mn/Si(111)-$\sqrt{3}\times\sqrt{3}$ surface has a similar surface reconstruction as the Ag/Si(111)-$\sqrt{3}\times\sqrt{3}$ case. A model of the top surface layer consisting of Mn and Si trimers is illustrated in Fig. 4(d), overlaid on the hexagonal STM image. White and black circles correspond to Mn and Si atoms, respectively. In this case the smaller Mn trimer should appear brighter in the STM image and is what we observe in Figs. 4(a) and 4(b). The honeycomb pattern seen in Fig. 4(c) can be explained by the observation of both the small and large Mn trimers. It should be noted that the suggestion in a very recent STM study (Ref. 8) that the protrusions in the hexagonal pattern correspond to Si trimers is not consistent with the observation of the honeycomb pattern of Fig. 4(c).

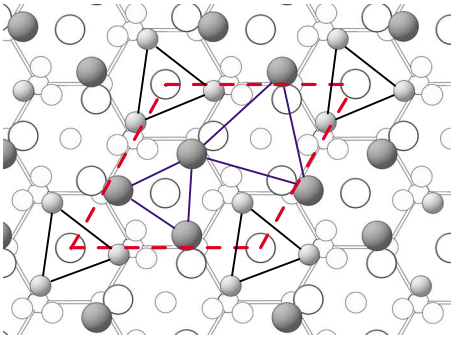

FIG. 5. (Color online) Top view of the atomic-structure model of the MnSi film with B20 structure according to Ref. 4. The $\sqrt{3}\times\sqrt{3}$ unit cell is indicated by the dashed line. Small light gray spheres (connected with black lines) represent Si atoms in the top-layer and large dark gray spheres (connected with blue lines) represent Mn atoms in the first Mn layer. The hexagonal bonding pattern displays the Si substrate lattice.

The location of the Si atoms in this model is not straightforward to determine experimentally since they are not observed in the STM images. This is also similar to the Ag/Si(111)-$\sqrt{3}\times\sqrt{3}$ case.[19] In the model presented in Fig. 4(d), the top Si layer is arranged into trimers, located between six Mn trimers and appearing as black holes in the STM images. This is consistent with the IET model as well as with a recent theoretical model as discussed below.

The above discussed surface atomic model fits very well to the atomic structure predicted by Hortamani *et al.*[4] Even though not discussed in detail in that study, the calculations predict a triangular arrangement of the top Mn and Si layers that is similar to the IET model of the Ag/Si(111)-$\sqrt{3}\times\sqrt{3}$ surface as seen in Fig. 1 of Ref. 4. This is further illustrated in Fig. 5, which shows a top view of the model of Ref. 4. In the figure, the top Mn and Si atoms are highlighted as well as the triangular structure. As seen, the top Mn atoms form chained triangles, two in each surface unit cell, with different size. In between, Si trimers are located in the corners of the unit cell. This is quite similar to the top layers of the IET model. A small difference can be observed compared to the Ag/Si(111)-$\sqrt{3}\times\sqrt{3}$ case: in the Mn-silicide structure the Si trimers are slightly above the Mn trimers,[4] (~0.5 Å) whereas in the Ag case the Ag trimers are above the Si trimers.[20] The Si termination of the Mn-silicide surface is supported by earlier photoemission studies. A strong surface component was seen in the Si $2p$ core-level spectra (S_3 in Ref. 15),[15,16] which indicated that the surface is terminated by Si atoms. The invisibility of the Si atoms in the STM images is thus an electronic effect, possibly caused by a higher binding energy of the Si orbitals. On the other hand, the strong visibility of the Mn trimers is consistent with

valence-band photoemission spectra,[15] which show a high intensity at the Fermi edge, implying that the Mn 3*d* states extend into the band gap. Theoretical modeling of STM images would be useful to shed more light on this issue.

The extra white protrusions that are observed on top of the $\sqrt{3}$ film are located in the middle between three small Mn trimers, i.e., on top of the large Mn trimer [assuming the model in Figs. 4(d) and 5]. The amount of extra protrusions at the 3 ML sample was ~7%. The extra protrusions have also been observed by Kumar *et al.*[16] but with a coverage of 20% and was interpreted as extra Si atoms due to a small low binding-energy feature in their Si 2*p* core-level spectra. In contrast to their conclusion, we suggest that these extra protrusions are Mn atoms for the following reasons. First, in our recent high-resolution Si 2*p* core-level study the small low binding-energy feature was interpreted as coming from the second Si layer.[15] Second, in the high-resolution STM image [Fig. 4(c)], the extra white protrusions have a diffuse appearance possibly caused by delocalized electronic states. Third, contamination from oxygen can be ruled out for the following reason: oxygen contaminations cannot have a threefolded symmetry. These three points suggest that the extra white protrusions are Mn atoms.

In order to obtain information about the change in electronic structure from the different surfaces, area averaged STS spectra were recorded. Figures 6(a)–6(f) show STS spectra recorded from the clean Si(111)-7×7 surface and the surfaces with different Mn coverages. The spectrum from the clean surface shows a peak at −0.3 eV, denoted A, corresponding to the filled adatom state and a broad feature, B, around −1.1 eV. The latter state is the contribution from both the rest atom and backbond states. Also, at ~0.55 eV above the Fermi level (at 0 eV), the empty adatom state is clearly shown (A^*). These states are consistent with those reported by Hamers *et al.*[21] and Wolkow *et al.*[22]

Spectrum (b) in Fig. 6 was measured on the as-deposited 1.5 ML surface. Three peaks are observed, two located at −0.55 and −1.7 eV below E_F and one located at 0.95 eV above the Fermi level. These states are considered to have its origin from the deposited Mn. The spectrum recorded from the 1×1 surface annealed at 300 °C is shown in spectrum (c) in Fig. 6. One new distinct peak is found, compared to spectrum (b), located at −1.3 eV. Also, one state is found at −0.6 eV. Overall, the peaks in the spectrum are located at similar energies as the peaks observed for the as-deposited sample. Apparently the electronic structure on both the as-deposited sample and after 300 °C anneal, is dominated by the unreacted Mn clusters seen in the STM images in Figs. 2(b) and 2(c).

Spectrum (d) in Fig. 6 is the area averaged STS spectrum recorded from the $\sqrt{3}$ islands in Fig. 2(e) (1.5 ML sample annealed at 400 °C). Four main peaks are observed, located at −0.4, −1.6, 0.7, and 2.2 eV, respectively. These are labeled as SS_1 and SS_2, (occupied states), and SS_1^* and SS_2^* (unoccupied states), respectively. The occupied state SS_1 cuts into the Fermi level and indicates that the $\sqrt{3}\times\sqrt{3}$ surface is metallic.

Spectrum (e) in Fig. 6 is the area averaged STS spectrum from the 3 ML $\sqrt{3}$ film. Three peaks are resolved, located −0.3, −1, and −2 eV, below the Fermi level. These are labeled as S_1, S_2, and S_3, respectively. Above the Fermi level three well-resolved surface-state features are also resolved and are labeled as S_1^*-S_3^*. Both the occupied state S_1 and the unoccupied state S_1^* cross the Fermi level and show that the surface is metallic. It is interesting to note that this spectrum shows similar surface states as those reported from our angle-resolved photoelectron spectroscopy (ARPES) study of the $\sqrt{3}$ surface.[15] The positions of the three filled states peaks in the STS spectrum agree with the energy positions of the five surface states in the ARPES study, which are at about −0.2, −0.4, −0.9, −1.1, and −1.9 eV below the Fermi level.

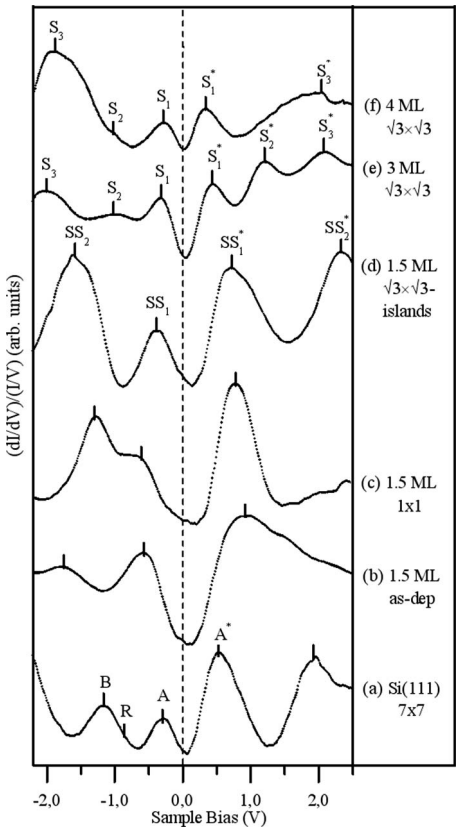

FIG. 6. Area averages STS spectra recorded from the (a) clean Si(111)-7×7 surface, (b) the 1.5 ML as-deposited film, (c) the 1.5 ML film annealed at 300 °C, (d) the 1.5 ML film annealed at 400 °C, (e) 3ML film annealed at 400 °C, and (f) the 4 ML film annealed at 400 °C.

Spectrum (f) in Fig. 6 was recorded from the 4 ML surface shown in Fig. 3(d), i.e., from the full $\sqrt{3}$ layer plus extra $\sqrt{3}$ islands. As expected, the spectrum is quite similar to the spectrum of the 3 ML $\sqrt{3}$ layer (e) with the surface states appearing at about the same energies. However, some differences in intensity are seen with peak S_2^* as a broad shoulder in spectrum (f).

The spectrum recorded from $\sqrt{3}$ islands for 1.5 ML coverage shows significant differences compared to the 3 and 4 ML spectra, recorded from large continuous $\sqrt{3}$ layers. The peaks from the $\sqrt{3}$ islands appear broader, split into two contributions, and seem slightly shifted in energy. The gap between the two peaks closest to the Fermi level, SS_1 and SS_1^*, is larger. Possibly this could be related to quantum-confinement effects.[23]

IV. CONCLUSION

In conclusion, the MnSi film formation and the surface atomic and electronic structure have been investigated in detail by STM/STS at Mn coverages between 1.5 and 12 ML. At a coverage of 1.5 ML island formation is favored while at 3 ML the Si substrate is almost fully covered with a well-ordered Mn-silicide film. Annealing the 1.5 ML sample at 450 °C results in a restored 7×7 surface together with large silicide islands. At a coverage of 4 ML the $\sqrt{3}$ MnSi silicide film totally covers the substrate. On top of the film islands are found which are also terminated with a well-ordered $\sqrt{3}\times\sqrt{3}$ surface. For higher coverages up to 12 ML, uniform film growth is found.

The STM images of the $\sqrt{3}$ MnSi silicide surface show both a hexagonal and a honeycomb pattern, depending on the tip condition. This is interpreted as arising from Mn atoms arranged in a triangular structure. A model for the MnSi silicide surface is proposed, which is similar to the top atomic layers of the IET model for the Si(111)$\sqrt{3}\times\sqrt{3}$-Ag surface. This is supported by a recent theoretical study.

High-resolution STS spectra have been presented for the different surfaces. The features observed in the STS spectra for the 3 and 4 ML surfaces show clear empty- and filled-state features. The filled-states are similar to those shown in earlier published ARPES studies.

ACKNOWLEDGMENTS

The authors would like to thank Peter Kratzer for valuable comments and for letting us use the image of the atomic structure. This work was supported by the National Research School in Materials Science and the Swedish Research Council.

*joakim.hirvonen@kau.se

[1] S. A. Wolf, D. D. Awschalom, R. A. Buhrman, J. M. Daughton, S. von Molnar, M. L. Roukes, A. Y. Chtchelkanova, and D. M. Treger, Science **294**, 1488 (2001).
[2] M. M. R. Evans, J. C. Glueckstein, and J. Nogami, Phys. Rev. B **53**, 4000 (1996).
[3] M. Tanaka, Q. Zhang, M. Takeguchi, and K. Furuya, Surf. Sci. **532-535**, 946 (2003).
[4] M. Hortamani, P. Kratzer, and M. Scheffler, Phys. Rev. B **76**, 235426 (2007).
[5] S. M. Shivaprasad, C. Anandan, S. G. Azatyan, Y. L. Gavriljuk, and V. G. Lifshits, Surf. Sci. **382**, 258 (1997).
[6] T. Nagao, S. Ohuchi, Y. Matsuoka, and S. Hasegawa, Surf. Sci. **419**, 134 (1999).
[7] S. Higashi, P. Kocán, and H. Tochihara, Phys. Rev. B **79**, 205312 (2009).
[8] S. Higashi, Y. Ikedo, P. Kocán, and H. Tochihara, Appl. Phys. Lett. **93**, 013104 (2008).
[9] G. Ctistis, U. Deffke, J. J. Paggel, and P. Fumagalli, J. Magn. Magn. Mater. **240**, 420 (2002).
[10] G. Ctistis, U. Deffke, K. Schwinge, J. J. Paggel, and P. Fumagalli, Phys. Rev. B **71**, 035431 (2005).
[11] K. Schwinge, J. J. Paggel, and P. Fumagalli, Surf. Sci. **601**, 810 (2007).
[12] K. H. Kim, S. W. Han, J. D. Lee, J. J. Lee, K. J. Kim, B. S. Kim, S. C. Wi, S. S. Lee, G. Kim, and J.-S. Kang, J. Korean Phys. Soc. **48**, 931 (2006).
[13] E. Magnano, E. Carleschi, A. Nicolaou, T. Pardini, M. Zangrando, and F. Parmigiani, Surf. Sci. **600**, 3932 (2006).
[14] E. Carleschi, E. Magnano, M. Zangrando, F. Bondino, A. Nicolaou, F. Carbone, D. Van der Marel, and F. Parmigiani, Surf. Sci. **601**, 4066 (2007).
[15] J. Hirvonen Grytzelius, H. M. Zhang, and L. S. O. Johansson, Phys. Rev. B **78**, 155406 (2008).
[16] A. Kumar, M. Tallarida, M. Hansmann, U. Starke, and K. Horn, J. Phys. D **37**, 1083 (2004).
[17] S. Azatyan, M. Hirai, M. Kusaka, and M. Iwami, Appl. Surf. Sci. **237**, 105 (2004).
[18] I. Horcas, R. Fernández, J. M. Gómez-Rodríguez, J. Colchero, J. Gómez-Herrero, and A. M. Baro, Rev. Sci. Instrum. **78**, 013705 (2007).
[19] H. M. Zhang, J. B. Gustafsson, L. S. O. Johansson, Phys. Rev. B **74**, 201304(R) (2006).
[20] H. Aizawa, M. Tsukada, N. Sato, and S. Hasegawa, Surf. Sci. **429**, L509 (1999).
[21] R. J. Hamers, R. M. Tromp, and J. E. Demuth, Phys. Rev. Lett. **56**, 1972 (1986).
[22] R. Wolkow and Ph. Avouris, Phys. Rev. Lett. **60**, 1049 (1988).
[23] E. A. Johnson, in *Low-Dimensional Semiconductor Structures*, edited by K. Barnham and D. Vvedensky (Cambridge University Press, Cambridge, 2001).